Acta Mech 231, 4077–4093 (2020)
https://doi.org/10.1007/s00707-020-02752-1

ORIGINAL PAPER

Kotaro Miura · **Makoto Sakamoto** · **Yuji Tanabe**

Analytical solution of axisymmetric indentation of multi-layer coating on elastic substrate body

Received: 24 December 2019 / Revised: 27 May 2020 / Published online: 8 July 2020

Abstract We consider the axisymmetric contact problem of a multi-elastic layer with various elastic constants bonded to an elastic semi-infinite substrate indented by rigid flat-ended cylindrical and spherical indenters. The transfer matrix method is applied to each elastic layer, and dual integral equations are reduced to an infinite system of simultaneous equations by expressing the normal contact stress at the surface elastic layer as an appropriate series with Chebyshev orthogonal polynomials. Numerical results demonstrate the effects of the elastic constant of each elastic layer and the semi-infinite elastic substrate on the radial distribution of the normal contact stress and normal displacement of the free surface of the elastic layer, stress singularity factor at the edge of the cylindrical indenter, and axial load of a rigid indenter which penetrates the multi-layer material to a constant depth. The results of axial load are in good agreement with previously reported results. The numerical results are given for several combinations of the shear modulus of each elastic layer and the substrate. These results will contribute to the establishment of indentation tests for composite materials and serve as guidelines for the design of appropriate mechanical properties of layered materials.

1 Introduction

Improvements in the stiffness of material surfaces are of great interest in the thin film and tribology fields. Indentation tests are widely used to measure the local mechanical properties of materials such as metal coating layers and biological tissues. However, the load–displacement curve obtained from indentation tests includes contributions from the material bulk, not only the surface, making it difficult to estimate the mechanical properties of the surface. Therefore, an understanding of the stress and displacement of layered materials is needed.

Indentation tests are based on a contact problem known as Boussinesq's problem. This problem for a semi-infinite space indented by conical, spherical, and flat-ended cylindrical indenters was solved by Harding and Sneddon [1], Sneddon [2], and Muki [3]. Lebedev and Ufliand [4] solved the contact problem for an elastic layer resting frictionlessly on a rigid foundation indented by a flat-ended cylindrical indenter by reducing the dual integral equations of stress and displacement to a single Fredholm integral equation of the second kind. Hayes et al. [5] solved the problem for an elastic layer bonded to a rigid foundation indented by flat-ended

K. Miura (✉)
Department of Systems Design Engineering, Seikei University, 3-3-1 Kichijojikitamachi, Musashino-shi, Tokyo 180-8633, Japan
E-mail: k_miura@st.seikei.ac.jp

M. Sakamoto
Department of Health Sciences, Niigata University School of Medicine, 2-746 Asahimachi, Niigata 951-8518, Japan

Y. Tanabe
Graduate School of Science and Technology, Niigata University, 2-8050, Niigata 950-2181, Japan

cylindrical and spherical indenters to provide an analytical method for evaluating the mechanical properties of articular cartilage bonded to the subchondral bone via indentation tests. They introduced an indentation scaling factor for considering the effect of layer thickness. Indentation scaling factors, commonly used in indentation testing to account for thickness or substrate effects, for a spherical indenter and a monomial blunt indenter were introduced for the asymptotic modeling approach by Argatov et al. [6] and Argatov and Sabina [7], respectively. Argatov and Sabina [7] used an indentation scaling factor for a cylindrical indenter to evaluate the incremental indentation stiffness for an arbitrary axisymmetric indenter that produces a circular area of contact. Dhaliwal [8] solved the axisymmetric contact problem for an elastic layer bonded to an elastic semi-infinite space indented by a flat-ended cylindrical indenter by reducing this boundary value problem to a single Fredholm integral equation of the second kind to estimate the safety of foundations supporting cylindrical columns. The indentation of an elastic layer perfectly bonded to an elastic substrate by flat-ended cylindrical, conical, and spherical indenters was considered by Yu et al. [9]. They showed that the axial load of the rigid indenter is related to layer thickness and the relative error between the axial load of the layered material and that of the semi-infinite space with the mechanical properties of an elastic surface layer and found the optimal conditions for accurately measuring the surface mechanical properties of coating materials via indentation tests. Korsunsky and Constantinescu [10] considered the contact problem of an elastic layer perfectly bonded to or freely sliding on an elastic substrate for blunted conical, flat-ended cylindrical, spherical, and conical indenters using the method proposed by Lebedev and Ufliand [4]. They proposed the optimal conditions for accurately measuring the mechanical properties of the surface elastic layer or substrate via indentation tests for each indenter type based on the apparent contact modulus. Keer et al. [11] solved the contact problem between two deformable bodies coated by an elastic surface layer by reducing dual integral equations to a single Fredholm integral equation. Sakamoto et al. [12] solved the axisymmetric contact problem of two deformable spheres coated by transversely isotropic elastic layer by reducing dual integral equations to an infinite system of simultaneous equations using the technique of expanding the normal contact stress to an infinite series.

Several approximate solutions have also been proposed for estimating the effect of an elastic substrate or a multi-layer structure. Gao et al. [13] obtained a perturbation solution for the indentation problem of a nonhomogeneous medium with piecewise constant or continuously varying moduli indented by a rigid cylindrical punch. The validity of the perturbation solutions was examined by a comparison with finite element method results. The results agreed when the elastic moduli of the specimen and substrate were similar. Argatov [14] obtained a high-order asymptotic solution of the axisymmetric unilateral contact problem for a spherical punch indenting an elastic layer attached to an elastic substrate in explicit form for estimating the substrate effect on a thin film in the indentation process. A comparison with the perturbation results reported by Gao et al. [13] demonstrated good agreement between the two asymptotic approaches in a sufficiently wide range of the relative stiffness ratio. Furthermore, the paper reported that the applicability of the asymptotic models is governed by the ratio of the diameter of the contact area to the specimen thickness.

The contact problem of layered materials and functionally graded materials (FGMs) has become increasingly important. Volkov et al. [15] provided an approximate analytical solution to the contact problem for a soft functionally graded layer that arbitrarily varies with depth indented by a circular indenter. The kernel transform of the integral equation was constructed numerically using the method of modeling functions. Selvadurai and Katebi [16] considered the adhesive contact problem for an incompressible elastic half-space under the assumption that the shear modulus varies exponentially with depth. They represented the contact stress distributions by discrete equivalent distributions to compute the integral equations numerically. Liu et al. [17–19] considered the axisymmetric contact problem of FGMs by adding a multi-layer coating whose mechanical properties vary linearly in each elastic layer to express arbitrarily varying mechanical properties; however, the Poisson's ratios for the coating and the half-space were limited to 1/3. They reduced this problem to a Cauchy singular integral equation by using the transfer matrix method and the Hankel integral transform technique. Liu and Xing [20] reconsidered the contact problem of FGMs without limiting Poisson's ratio. Constantinescu et al. [21] extended the problem considered by Korsunsky and Constantinescu [10] to the axisymmetric indentation problem for a multi-layer elastic coating on an elastic substrate. They computed transfer matrices derived from the continuous interface condition of the stress and displacement symbolically in the software Mathematica. The Mathematica code for calculating the apparent contact modulus for various indenter types is available in their paper. Wei et al. [22] studied a laminate composed of multiple orthotropic rectangular layers with a viscoelastic adhesive at the interface subjected to a sinusoidal pressure at its top surface using the state-space method and transfer matrix method.

Recently, Ai and Zhang [23] solved the problem of a rigid rectangular plate on a transversely isotropic multi-layer medium in Cartesian coordinates using the double Fourier transform, Laplace transform, and transfer matrix method. They compared their numerical results with those obtained from the finite element method software ABAQUS. Stan and Adams [24] solved the adhesive contact problem of an elastic multi-layer coated substrate indented by a rigid spherical indenter using the transfer matrix method and the Hankel transform. Zhang et al. [25] considered the thermoplastic contact problem of multi-layer materials under friction heating.

Miura et al. [26] obtained an analytical solution for the axisymmetric contact problem for an elastic layer perfectly bonded to an elastic semi-infinite solid indented by flat-ended cylindrical and spherical indenters using a method that expresses the normal contact stress at the upper surface elastic layer as an appropriate series with Chebyshev orthogonal polynomials and by reducing the dual integral equations of stress and displacement to an infinite system of simultaneous equations, instead of a single Fredholm integral equation of the second kind. Their analytical method can be applied to various problems, such as crack problems [27] and the contact problem of two deformable bodies [12].

The present study considers the axisymmetric contact problem for a multi-layer material with various elastic modulus values in each layer bonded to an elastic semi-infinite solid indented by flat-ended cylindrical and spherical indenters. This contact problem is reduced to an infinite system of simultaneous equations using the method presented by Miura et al. [26], and the transfer matrices are derived from the continuous interface conditions of stress and displacement, as done by Liu and Xing [20]. The analytical solution provided here is exact because there is no approximation in the analysis procedure. The presented numerical results include not only the axial load which is important for evaluating the mechanical properties from the load–displacement curve obtained from indentation tests, but also the distribution of the normal contact stress below flat-ended cylindrical and spherical indenters, the distribution of the normal displacement at the upper surface of the elastic layer, and the stress singularity factor, which reveals the magnitude of the normal contact stress singularity at the edge of the flat-ended cylindrical punch. The axial load results are validated by a comparison to those calculated using the Mathematica code provided by Constantinescu et al. [21].

2 Problem formulation

Consider the problem of a composite material consisting of an arbitrary number of elastic layers perfectly bonded to an elastic semi-infinite substrate indented by a rigid flat-ended cylindrical or spherical indenter, as shown in Figs. 1 and 2. A cylindrical coordinate system (r, θ, z) is used in this study. The displacement components along r, θ, and z are denoted by u_r, v_θ, and w_z, respectively. The components of the stress tensor are σ_r, σ_θ, σ_z, $\tau_{r\,z}$, $\tau_{\theta\,z}$, and $\tau_{r\theta}$. A general solution of the equilibrium equations for the elastic layers and substrate without torsion can be derived using harmonic stress functions φ_0 and φ_3, i.e., [28]

$$2G_j u_r^{(j)} = \frac{\partial \varphi_0^{(j)}}{\partial r} + z\frac{\partial \varphi_3^{(j)}}{\partial r},$$

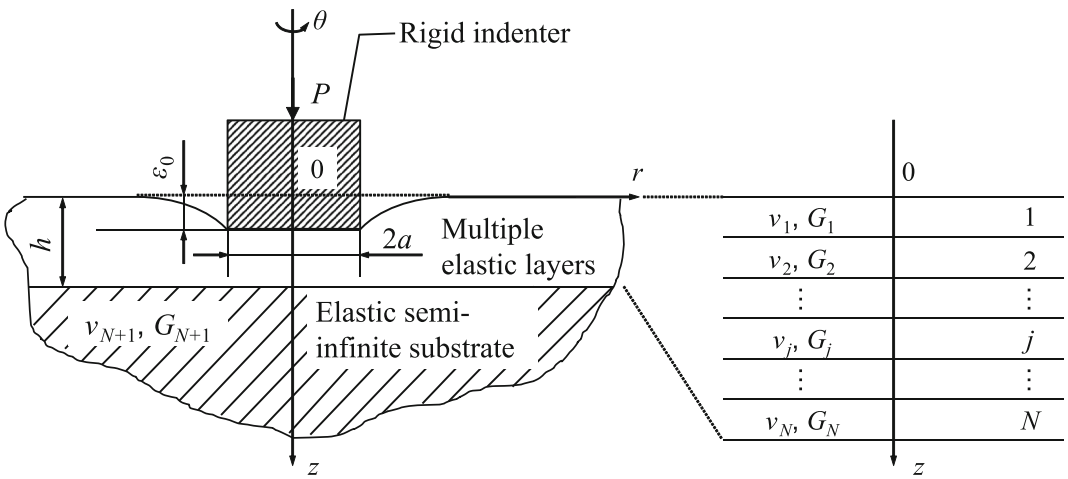

Fig. 1 Indentation of elastic multi-layer coating perfectly bonded to an elastic semi-infinite substrate

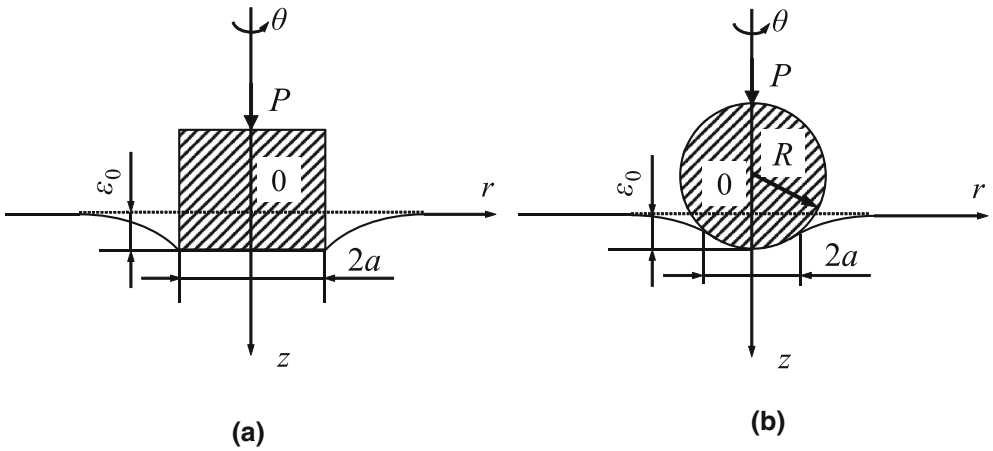

Fig. 2 Shape of axisymmetric indenter: **a** rigid cylindrical indenter and **b** rigid spherical indenter

$$
\begin{aligned}
v_\theta^{(j)} &= 0,\\
2G_j w_z^{(j)} &= \frac{\partial \varphi_0^{(j)}}{\partial z} + z\frac{\partial \varphi_3^{(j)}}{\partial z} - (3-4\nu_j)\varphi_3^{(j)},\\
\sigma_r^{(j)} &= \frac{\partial^2 \varphi_0^{(j)}}{\partial r^2} + z\frac{\partial^2 \varphi_3^{(j)}}{\partial r^2} - 2\nu_j\frac{\partial \varphi_3^{(j)}}{\partial z},\\
\sigma_\theta^{(j)} &= \frac{\partial \varphi_0^{(j)}}{r\partial r} + z\frac{\partial \varphi_3^{(j)}}{r\partial r} - 2\nu_j\frac{\partial \varphi_3^{(j)}}{\partial z},\\
\sigma_z^{(j)} &= \frac{\partial^2 \varphi_0^{(j)}}{\partial z^2} + z\frac{\partial^2 \varphi_3^{(j)}}{\partial z^2} - 2(1-\nu_j)\frac{\partial \varphi_3^{(j)}}{\partial z},\\
\tau_{rz}^{(j)} &= \frac{\partial^2 \varphi_0^{(j)}}{\partial r\partial z} + z\frac{\partial^2 \varphi_3^{(j)}}{\partial r\partial z} - (1-2\nu_j)\frac{\partial \varphi_3^{(j)}}{\partial r},\\
\tau_{r\theta}^{(j)} &= \tau_{\theta z}^{(j)} = 0, \quad (j = 1, 2, \ldots, N+1),
\end{aligned}
\tag{1}
$$

where the superscript j represents the number of elastic layers and $j = N+1$ represents the elastic semi-infinite substrate. G_j and ν_j denote the shear modulus and Poisson's ratio, respectively, of each elastic layer and the substrate. The harmonic functions $\varphi^{(j)_0}$ and $\varphi^{(j)_3}$ for the elastic layers can be written as

$$
\begin{cases}
\varphi_0^{(j)} = \int_0^\infty \left\{D^{(j)}(\lambda)\cosh\lambda z + A^{(j)}(\lambda)\sinh\lambda z\right\} J_0(\lambda r)\mathrm{d}\lambda,\\
\varphi_3^{(j)} = \int_0^\infty \left\{B^{(j)}(\lambda)\sinh\lambda z + C^{(j)}(\lambda)\cosh\lambda z\right\} J_0(\lambda r)\mathrm{d}\lambda,
\end{cases}
\quad (j = 1, 2, \ldots, N), \tag{2}
$$

and those for the elastic substrate can be written as

$$
\begin{aligned}
\varphi_0^{(N+1)} &= \int_0^\infty A^{(N+1)}(\lambda) J_0(\lambda r) e^{-\lambda z}\mathrm{d}\lambda,\\
\varphi_3^{(N+1)} &= \int_0^\infty B^{(N+1)}(\lambda) J_0(\lambda r) e^{-\lambda z}\mathrm{d}\lambda,
\end{aligned}
\tag{3}
$$

where $J_n(\lambda r)$ is the Bessel function of the first kind of order n and $A^{(j)}(\lambda)$, $B^{(j)}(\lambda)$, $C^{(j)}(\lambda)$, $D^{(j)}(\lambda)$, $A^{(N+1)}(\lambda)$, and $B^{(N+1)}(\lambda)$ are unknown functions that can be obtained by matching appropriate boundary conditions.

If the shear traction between the indenter and each layer is assumed to be negligible, then the boundary conditions of the upper surface of the layer can be described by the following equations:

$$
(w_z)_{z=0}^{(1)} = \varepsilon_0 - f(r), \quad (0 \le r \le a), \tag{4}
$$

$$(\sigma_z)^{(1)}_{z=0} = 0, \quad (a < r < \infty), \tag{5}$$

$$(\tau_{rz})^{(1)}_{z=0} = 0, \quad (0 \le r < \infty). \tag{6}$$

Under the condition of Eq. (4), for the cylindrical indenter, the normal displacement at contact area between the indenter and a layer is equal to the penetration depth ε_0, and thus, $f(r) = 0$. For the spherical indenter, the normal displacement varies at the contact area, and thus, the function $f(r)$ related to the geometry of the indenter-layer interface is required.

The elastic layer is perfectly bonded to the next elastic layer or the semi-infinite substrate; therefore, the continuity conditions of the components of displacement and traction at the interface between an elastic layer and the next layer or the semi-infinite substrate, represented by $z = h_j$ can be written in the following form:

$$\left[\left\{S^{(j)}\right\} = \left\{S^{(j+1)}\right\}\right]_{z=h_j}, \quad (j = 1, 2, \ldots, N), \tag{7}$$

where

$$\left\{S^{(j)}\right\} = \left[\begin{array}{cccc} u_r^{(j)} & w_z^{(j)} & \sigma_z^{(j)} & \tau_{rz}^{(j)} \end{array}\right]^T. \tag{8}$$

By substituting Eqs. (2) and (3) into the equilibrium equations (1), the components of displacement and traction are expressed in the form of the Hankel transform as follows:

$$\begin{aligned} u_r^{(j)} &= \frac{1}{2G_j}\int_0^\infty \zeta_r^{(j)}(\lambda, z) J_1(\lambda r)\mathrm{d}\lambda, \\ w_z^{(j)} &= \frac{1}{2G_j}\int_0^\infty \zeta_z^{(j)}(\lambda, z) J_0(\lambda r)\mathrm{d}\lambda, \\ \sigma_z^{(j)} &= \int_0^\infty \xi_z^{(j)}(\lambda, z)\lambda J_0(\lambda r)\mathrm{d}\lambda, \\ \tau_{rz}^{(j)} &= \int_0^\infty \xi_{rz}^{(j)}(\lambda, z)\lambda J_1(\lambda r)\mathrm{d}\lambda. \end{aligned} \tag{9}$$

The functions $\zeta^{(j)_r}$, $\zeta^{(j)_z}$, $\xi^{(j)_z}$, and $\xi^{(j)_{rz}}$ are related to λ, which is a variable of the Hankel transform, and the displacement in the z-direction. They are summarized as a matrix in the following form:

$$\left\{\bar{S}^{(j)}(\lambda, z)\right\} = \left[\begin{array}{cccc} \zeta_r^{(j)}(\lambda, z) & \zeta_z^{(j)}(\lambda, z) & \xi_z^{(j)}(\lambda, z) & \xi_{rz}^{(j)}(\lambda, z) \end{array}\right]^T = \left[L_j(\lambda, z)\right]\left\{A_j(\lambda)\right\}, \tag{10}$$

where

$$\left[L_j(\lambda, z)\right] = \left[\begin{array}{cccc} -\frac{\sinh\lambda z}{2G_j} & -\frac{z\lambda\sinh\lambda z}{2G_j} & -\frac{z\lambda\cosh\lambda z}{2G_j} & -\frac{\cosh\lambda z}{2G_j} \\ \frac{\cosh\lambda z}{2G_j} & \frac{z\lambda\cosh\lambda z - (3-4\nu_j)\sinh\lambda z}{2G_j} & \frac{z\lambda\sinh\lambda z - (3-4\nu_j)\cosh\lambda z}{2G_j} & \frac{\sinh\lambda z}{2G_j} \\ \sinh\lambda z & z\lambda\sinh\lambda z - 2(1-\nu_j)\cosh\lambda z & z\lambda\cosh\lambda z - 2(1-\nu_j)\sinh\lambda z & \cosh\lambda z \\ -\cosh\lambda z & -z\lambda\cosh\lambda z + (1-2\nu_j)\sinh\lambda z & -z\lambda\sinh\lambda z + (1-2\nu_j)\cosh\lambda z & -\sinh\lambda z \end{array}\right], \tag{11}$$

$$\left\{A_j(\lambda)\right\} = \left[\begin{array}{cccc} \lambda A^{(j)}(\lambda) & B^{(j)}(\lambda) & C^{(j)}(\lambda) & \lambda D^{(j)}(\lambda) \end{array}\right]^T, \quad (j = 1, 2, \ldots, N).$$

For the case of an elastic semi-infinite substrate ($j = N+1$),

$$\left[L_{N+1}(\lambda, z)\right] = \left[\begin{array}{cc} -\frac{e^{-\lambda z}}{2G_{N+1}} & -\frac{\lambda z e^{-\lambda z}}{2G_{N+1}} \\ -\frac{e^{-\lambda z}}{2G_{N+1}} & -\frac{\{\lambda z + (3-4\nu_{N+1})\}e^{-\lambda z}}{2G_{N+1}} \\ e^{-\lambda z} & \{\lambda z + 2(1-\nu_{N+1})\}e^{-\lambda z} \\ e^{-\lambda z} & \{\lambda z + (1-2\nu_{N+1})\}e^{-\lambda z} \end{array}\right], \tag{12}$$

$$\{A_{N+1}(\lambda)\} = \left[\begin{array}{cc} \lambda A^{(N+1)} & B^{(N+1)} \end{array}\right]^T.$$

The continuity conditions in Eq. (7) lead to the following equations:

$$\left[\left\{\bar{S}^{(j)}\right\} = \left\{\bar{S}^{(j+1)}\right\}\right]_{z=h_j}, \quad (j = 1, 2, \ldots, N). \tag{13}$$

Substituting Eq. (10) into Eq. (13) yields the following equation related to an arbitrary elastic layer:

$$\left\{A_j(\lambda)\right\} = \left[V_j(\lambda, h_j)\right]\left\{A_{j+1}(\lambda)\right\}, \tag{14}$$

where $[V_j(\lambda, h_j)] = [L_j(\lambda, h_j)]^{-1}\,[L_{j+1}(\lambda, h_j)]$ is the transfer matrix, which gives the relationship between an arbitrary elastic layer and the next layer.

According to Eq. (13), Eq. (14) can be applied iteratively until it reaches the semi-infinite substrate, and thus,

$$\left\{A_j(\lambda)\right\} = \left[\hat{V}_j(\lambda, h_j, \ldots, h_N)\right]\{A_{N+1}(\lambda)\}, \tag{15}$$

where

$$\left[\hat{V}_j(\lambda, h_j, \ldots, h_N)\right] = \left[V_j(\lambda, h_j)\right]\left[V_{j+1}(\lambda, h_{j+1})\right]\ldots[V_N(\lambda, h_N)]. \tag{16}$$

From the boundary condition (6), we can obtain the following equation:

$$\lambda A^{(1)}(\lambda) = (1 - 2\nu_1)C^{(1)}(\lambda). \tag{17}$$

Applying Eq. (17) to the relationship between the top surface layer and the semi-infinite substrate obtained from Eq. (15) yields the following equation:

$$\{A_{N+1}(\lambda)\} = \left\{[B]\left[\hat{V}_1(\lambda, h_1, \ldots, h_N)\right]\right\}^{-1}\begin{bmatrix}1-2\nu_1\\1\end{bmatrix}C^{(1)}(\lambda), \tag{18}$$

where

$$[B] = \begin{bmatrix}1 & 0 & 0 & 0\\ 0 & 0 & 1 & 0\end{bmatrix}. \tag{19}$$

Equation (18) indicates that the unknown functions $A^{(j)}(\lambda)$, $B^{(j)}(\lambda)$, $C^{(j)}(\lambda)$, $D^{(j)}(\lambda)$, $A^{(N+1)}(\lambda)$, and $B^{(N+1)}(\lambda)$ can be reduced to the unknown function $C^{(j)}(\lambda)$.

The normal stress of the top surface layer $(\sigma_z)^{(1)_{z=0}}$ can be written as the following equation related to $C^{(1)}(\lambda)$ by substituting Eqs. (15) and (18) into $\xi^{(1)_z}(\lambda, 0)$ in Eq. (10):

$$(\sigma_z)^{(1)}_{z=0} = \int_0^\infty M(\lambda, h_1, \ldots, h_N)C^{(1)}(\lambda)\lambda J_0(\lambda r)\mathrm{d}\lambda, \tag{20}$$

where

$$M(\lambda, h_1, \ldots, h_N) = [B_1]\,[L_1(\lambda, 0)]\left[\hat{V}_1(\lambda, h_1, \ldots, h_N)\right]\left\{[B]\left[\hat{V}_1(\lambda, h_1, \ldots, h_N)\right]\right\}^{-1}\begin{bmatrix}1-2\nu_1\\1\end{bmatrix}, \tag{21}$$

$$[B_1] = \begin{bmatrix}0 & 0 & 1 & 0\end{bmatrix}. \tag{22}$$

Eventually, the normal displacement of the surface of the top layer $(w_z)^{(1)_{z=0}}$ and the contact stress $(\sigma_z)^{(1)_{z=0}}$ can be written as the following equations, which contain only unknown function $C^{(j)}(\lambda)$ and apply the boundary conditions in Eqs. (4) and (5):

$$(w_z)^{(1)}_{z=0} = -\frac{1-\nu_1}{G_1}\int_0^\infty C^{(1)}(\lambda)J_0(\lambda r)\mathrm{d}\lambda = \varepsilon_0 - f(r), \quad (0 \le r < a), \tag{23}$$

$$(\sigma_z)^{(1)}_{z=0} = \int_0^\infty M(\lambda, h_1, \ldots, h_N)C^{(1)}(\lambda)\lambda J_0(\lambda r)\mathrm{d}\lambda = 0, \quad (a < r < \infty). \tag{24}$$

The dual integral equations [Eqs. (23) and (24)] are the typical form of a mixed boundary-value contact problem. In this study, the normal contact stress between the indenter and the layer surface is expressed as an appropriate series function that contains Chebyshev polynomials $T_n(x)$. The Hankel inversion is also applied to reduce the problem to an infinite system of simultaneous equations [26].

The normal contact stress is expressed using Chebyshev polynomials as

$$(\sigma_z)^{(1)}_{z=0} = \frac{2}{\pi r(a^2 - r^2)^{1/2}} \sum_{n=0}^{\infty} x_n T_{2n+1}(r/a), \quad (0 \le r < a), \tag{25}$$

where x_n $(n = 0, 1, 2, \ldots)$ are unknown coefficients. Using the entity [29]

$$\int_0^{\infty} \lambda Z_n(\lambda) J_0(\lambda r)\, \mathrm{d}\lambda = \begin{cases} 0, & (a < r < \infty), \\ \frac{2T_{2n+1}(r/a)}{\pi r(a^2 - r^2)^{1/2}}, & (0 \le r < a), \end{cases} \tag{26}$$

where

$$Z_n(\lambda) = J_{n+1/2}(\frac{\lambda a}{2}) J_{-n-1/2}(\frac{\lambda a}{2}), \quad (n = 0, 1, 2, \ldots), \tag{27}$$

the Hankel inversion is applied to Eqs. (24) and (25), and $C^{(j)}(\lambda)$ can be rewritten as the following equation by considering equalization of both equations:

$$C^{(1)}(\lambda) = p(\lambda, h_1, \ldots, h_N) \sum_{n=0}^{\infty} x_n(\lambda) Z_n(\lambda), \tag{28}$$

where

$$p(\lambda, h_1, \ldots, h_N) = 1/M(\lambda, h_1, \ldots, h_N). \tag{29}$$

Substituting Eq. (28) into Eq. (23) and using Gegenbauer's formula [30]

$$J_0(\lambda r) = \sum_{m=0}^{\infty} (2 - \delta_{0m}) X_m(\lambda) \cos m\phi, \quad (r = a\sin(\phi/2)), \tag{30}$$

we obtain

$$\sum_{n=0}^{\infty} x_n \int_0^{\infty} p(\lambda, h_1, \ldots, h_N) Z_n(\lambda) \sum_{m=0}^{\infty} (2 - \delta_{0m}) X_m(\lambda) \cos m\phi\, \mathrm{d}\lambda = \frac{G_1}{1 - \nu_1} \{-\varepsilon_0 + f(r)\}, \quad (0 \le r \le a), \tag{31}$$

where δ_{0m} is the Kronecker delta function and

$$X_m(\lambda) = J_m^2(\lambda a/2), \quad (m = 0, 1, 2, \ldots). \tag{32}$$

The function $f\,(r)$ depends on the shape of the indenter; therefore, the following equations were separated for cylindrical and spherical indenters. For the cylindrical indenter, $f\,(r)$ is simply zero. For a spherical indenter of radius R, the shape of the spherical indenter $f\,(r)$ to the first significant order of approximation is given by

$$f(r) \approx r^2/2R. \tag{33}$$

The following infinite system of simultaneous equations is then obtained from Eq. (31) for a cylindrical indenter:

$$\sum_{n=0}^{\infty} b_n A_{mn} = \delta_{0m}, \quad (m = 0, 1, 2, \ldots), \tag{34}$$

where

$$b_n = -\frac{1 - \nu_1}{G_1 \varepsilon_0} x_n, \tag{35}$$

$$A_{mn} = \int_0^{\infty} p(\lambda, h_1, \ldots, h_N) X_m(\lambda) Z_n(\lambda) \mathrm{d}\lambda. \tag{36}$$

For a spherical indenter,

$$\sum_{n=0}^{\infty} (b_n, c_n) A_{mn} = (\delta_{0m}, \delta_{1m}/2), \quad (m = 0, 1, 2, \ldots), \tag{37}$$

where

$$-\varepsilon_0 b_n + \frac{a^2}{4R} c_n = \frac{1-\nu_1}{G_1} x_n. \tag{38}$$

For a spherical indenter, the contact stress $(\sigma_z)^{(1)_{z=0}}$ approaches zero as $r \to \quad a-0$, and thus, we obtain

$$\frac{a^2}{4R\varepsilon_0} = \sum_{n=0}^{\infty} b_n / \sum_{n=0}^{\infty} c_n = \eta. \tag{39}$$

To calculate the infinite system of simultaneous equations in Eqs. (34) and (37), it is necessary to accurately evaluate the integration of A_{mn}. The details of this integration can be found in a previous study [26].

The numerical results for stress, displacement, and axial load can be obtained by calculating the coefficients b_n and c_n for cylindrical and spherical indenters in Eqs. (34) and (37), respectively. The normal contact stress $(\sigma_z)^{(1)}_{z=0}$ for a cylindrical indenter can be written in the form

$$(\sigma_z)^{(1)}_{z=0} = -\frac{2G_1\varepsilon_0}{(1-\nu_1)\pi r\sqrt{a^2-r^2}} \sum_{n=0}^{\infty} b_n T_{2n+1}\left(\frac{r}{a}\right), \quad (0 \le r < a), \tag{40}$$

and that for a spherical indenter can be expressed as

$$(\sigma_z)^{(1)}_{z=0} = -\frac{2G_1\varepsilon_0}{(1-\nu_1)\pi r\sqrt{a^2-r^2}} \sum_{n=0}^{\infty} (b_n - \eta c_n)\, T_{2n+1}\left(\frac{r}{a}\right), \quad (0 \le r < a). \tag{41}$$

The axial load P, obtained by integrating $(\sigma_z)^{(1)_{z=0}}$ over the contact area, for a cylindrical indenter is

$$P = -\frac{4G_1\varepsilon_0}{1-\nu_1} \sum_{n=0}^{\infty} \frac{(-1)^n}{2n+1} b_n, \tag{42}$$

and that for a spherical indenter is

$$P = -\frac{4G_1\varepsilon_0}{1-\nu_1} \sum_{n=0}^{\infty} \frac{(-1)^n}{2n+1} (b_n - \eta c_n). \tag{43}$$

The normal displacement $(w_z)^{(1)_{z=0}}$ for a cylindrical indenter and that for a spherical indenter can be represented, respectively, in the following forms:

$$\begin{aligned} \frac{(w_z)^{(1)}_{z=0}}{\varepsilon_0} = \sum_{n=0}^{\infty} b_n \Bigg[& \int_0^{\infty} \{p(\lambda, h_1, \ldots, h_N) - 1\}\, Z_n(\lambda) J_0(\lambda r) \mathrm{d}\lambda \\ & + \int_0^{\infty} \left\{ Z_n(\lambda) - \frac{2}{\pi\lambda a} \sin\lambda a \right\} J_0(\lambda r) \mathrm{d}\lambda \\ & + \frac{2}{\pi a} \left\{ H(a-r)\frac{\pi}{2} + H(r-a)\sin^{-1}\left(\frac{a}{r}\right) \right\} \Bigg], \end{aligned} \tag{44}$$

and

$$\begin{aligned} \frac{(w_z)^{(1)}_{z=0}}{\varepsilon_0} = \sum_{n=0}^{\infty} (b_n - \eta c_n) \Bigg[& \int_0^{\infty} \{p(\lambda, h_1, \ldots, h_N) - 1\}\, Z_n(\lambda) J_0(\lambda r) \mathrm{d}\lambda \\ & + \int_0^{\infty} \left\{ Z_n(\lambda) - \frac{2}{\pi\lambda a} \sin\lambda a \right\} J_0(\lambda r) \mathrm{d}\lambda \\ & + \frac{2}{\pi a} \left\{ H(a-r)\frac{\pi}{2} + H(r-a)\sin^{-1}\left(\frac{a}{r}\right) \right\} \Bigg], \end{aligned} \tag{45}$$

where $H(x)$ is the Heaviside unit step function. In this study, the stress singularity factor S is defined by the following equation to estimate the magnitude of the normal contact stress singularity at the edge of the cylindrical punch:

$$S = \lim_{r \to a-0} \sqrt{2\pi(a-r)}(\sigma_z)^{(1)}_{z=0}. \tag{46}$$

Substituting Eq. (40) into Eq. (46) yields

$$S = -\frac{2G_1\varepsilon_0}{(1-\nu_1)a\sqrt{\pi a}} \sum_{n=0}^{\infty} b_n. \tag{47}$$

3 Numerical results and discussion

Tables 1 and 2 show the convergence of coefficients b_n and c_n in an infinite system of simultaneous equations (Eqs. (34) and (37)). The number of elastic layers $N = 4$. The following numerical results in this section describe the mechanical properties of multiple elastic layers and a semi-infinite substrate under specific conditions. The Poisson's ratios ν_j of the elastic layers and semi-infinite substrate are all fixed at 0.3. This was done because the numerical results are not sensitive to the effect of Poisson's ratio; the effect of the shear moduli of the layer and substrate is dominant. Two systems are used for the shear moduli G_j. In the hard-coating system, the shear modulus increases linearly from the substrate to the surface layer, and in the soft-coating system, the shear modulus decreases linearly from the substrate to the surface layer as shown in Fig. 3

The number of coefficients b_n and c_n in this study was set to ten, which converged sufficiently. As shown in Tables 1 and 2, the convergence of coefficients decreased with decreasing aspect ratio h/a, which represents the total thickness of an elastic layer per radius of contact area. The fluctuation of coefficient values was close to zero when $h/a = 0.5$. However, the fluctuation is a trivial problem because it was near zero. The following discussion in this section compares the present results of axial load P to those reported by Constantinescu et al. [21]. The convergence of coefficients b_n and c_n is important for the accuracy of the numerical calculation because the numerical results are based on these coefficients.

Figure 4 shows the radial distribution of the normalized normal contact stress at the surface layer $(\sigma_z^*)^{(1)_{z=0}}$ below cylindrical and spherical indenters with respect to the normalized radial distance r/a for the hard-

Table 1 Convergence of b_n coefficients for various values of total layer thickness ratio h/a for a cylindrical indenter

n	h/a			
	0.5	1.0	1.5	2.0
Hard coating				
0	2.959360E−01	3.489798E−01	3.914975E−01	4.304908E−01
1	1.173272E−01	1.049666E−01	8.045479E−02	6.089026E−02
2	4.301099E−02	1.185515E−02	2.874942E−03	6.982334E−05
3	5.857748E−03	− 1.306166E−03	− 1.876149E−03	− 8.424862E−04
4	− 3.231934E−04	− 1.404621E−03	2.100388E−04	1.202193E−04
5	− 1.224493E−03	3.983458E−04	− 6.844856E−06	− 9.428652E−06
6	− 9.609879E−04	− 3.601073E−05	− 7.375190E−07	4.954441E−07
7	− 7.393853E−05	− 2.418956E−06	1.120215E−07	− 1.893079E−08
8	4.466071E−04	1.073306E−06	− 7.900570E−09	5.523234E−10
9	2.402032E−04	− 1.694065E−07	3.904331E−10	− 1.296039E−11
Soft coating				
0	2.667502E+00	2.208116E+00	1.942199E+00	1.768211E+00
1	− 6.479740E−01	− 4.301118E−01	− 2.861665E−01	− 1.966114E−01
2	− 1.457135E−01	− 2.656089E−02	3.519780E−03	8.912433E−03
3	− 1.158267E−02	1.103961E−02	5.779219E−03	1.910421E−03
4	1.050363E−02	3.303346E−03	− 4.423139E−04	− 3.707698E−04
5	6.984159E−03	− 3.374915E−04	− 9.323480E−05	3.391287E−05
6	1.789196E−03	− 5.134618E−04	2.440585E−05	− 2.047267E−06
7	− 4.158606E−04	2.180246E−04	− 2.864848E−06	9.042202E−08
8	− 8.773915E−04	− 4.741338E−05	2.219517E−07	− 3.080570E−09
9	− 5.172693E−04	7.790779E−06	− 1.325451E−08	8.555513E−11

Number of layers $N = 4$

Table 2 Convergence of $b_n/\eta - c_n$ coefficients for various values of total layer thickness ratio h/a for a spherical indenter

n	h/a			
	0.5	1.0	1.5	2.0
Hard coating				
0	8.350263E−01	1.179486E+00	1.433610E+00	1.602688E+00
1	−7.047671E−01	−1.088298E+00	−1.375389E+00	−1.564545E+00
2	−1.108010E−01	−8.810067E−02	−5.895514E−02	−4.038186E−02
3	−1.794534E−02	−4.223892E−03	−1.051035E−04	2.269766E−03
4	−1.645076E−03	6.512338E−04	9.864696E−04	−2.539432E−05
5	−1.101596E−04	7.055252E−04	−1.612670E−04	−6.482247E−06
6	2.890478E−04	−2.638139E−04	1.511491E−05	5.840804E−07
7	4.378653E−04	4.924052E−05	−9.836909E−07	−2.839021E−08
8	−6.727601E−05	−6.146996E−06	4.794215E−08	9.556387E−10
9	−4.173236E−04	6.093229E−07	−1.882479E−09	−2.473511E−11
Soft coating				
0	4.609345E+00	3.450469E+00	2.934960E+00	2.645922E+00
1	−5.164063E+00	−3.745472E+00	−3.109085E+00	−2.755628E+00
2	4.788556E−01	2.835842E−01	1.782514E−01	1.188943E−01
3	6.692432E−02	1.773388E−02	−7.049052E−04	−9.563807E−03
4	1.050958E−02	−3.949268E−03	−4.100776E−03	3.762585E−04
5	2.855177E−05	−3.636882E−03	7.510717E−04	−1.940117E−07
6	−2.552783E−03	1.550272E−03	−7.654282E−05	−8.131334E−07
7	−2.953194E−03	−3.176820E−04	5.352209E−06	5.026694E−08
8	8.140945E−04	4.303661E−05	−2.785933E−07	−1.830220E−09
9	3.091454E−03	−4.629800E−06	1.166613E−08	4.870771E−11

Number of layers $N = 4$

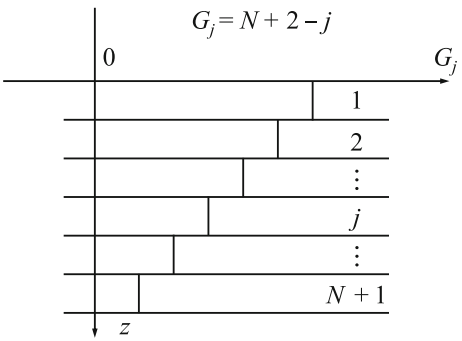

(a)

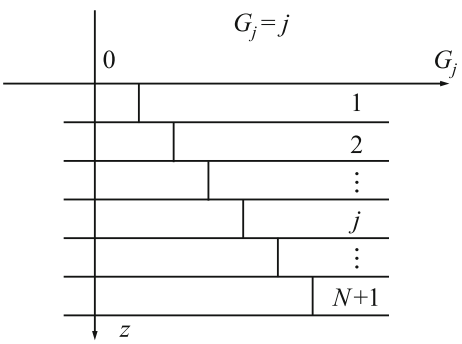

(b)

Fig. 3 Mechanical properties of elastic layers and semi-infinite substrate for **a** hard-coating system and **b** soft-coating system

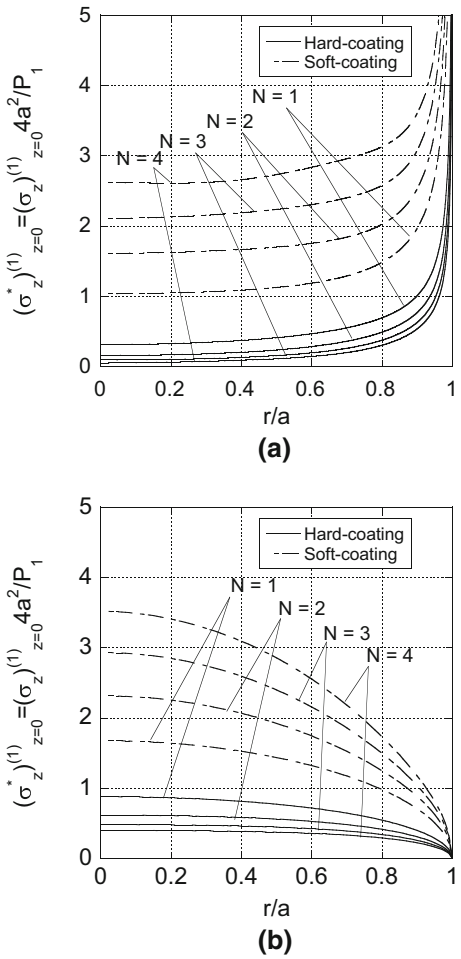

Fig. 4 Radial distribution of $(\sigma_z^*)_{z=0}^{(1)} = (\sigma_z)_{z=0}^{(1)} 4a^2/P_1$ in contact area $2a$ with respect to r/a below **a** flat-ended cylindrical indenter and **b** spherical indenter ($\nu_1 = \cdots = \nu_{N+1} = 0.3$, $h/a = 1.0$)

and soft-coating systems defined in Fig. 3. The aspect ratio h/a is fixed at 1.0 and the number of elastic layers $N = 1, 2, 3$, and 4. $(\sigma_z^*)^{(1)z=0}$ is normalized with respect to $P_1/4a^2$, where P_1 represents the axial load required for the cylindrical indenter to penetrate a given depth ε_0 into a homogeneous semi-infinite solid with the mechanical properties of the surface elastic layer. As shown in Fig. 4, the normal contact stress $(\sigma_z^*)^{(1)z=0}$ below the cylindrical indenter is at its minimum value at $r/a = 0$, and then increases and tends to infinity as $r \to a - 0$ because the edge of the cylindrical punch causes a stress singularity. For the spherical indenter, $(\sigma_z^*)_{z=0}^{(1)}$ below the indenter is maximum at the tip of the indenter and then decays to 0 as $r \to a - 0$ because the contact between the spherical indenter and the elastic layer smoothly ends at the edge of the contact area. The magnitude of $(\sigma_z^*)_{z=0}^{(1)}$ in the soft-coating system is higher than that in the hard-coating system because $(\sigma_z^*)_{z=0}^{(1)}$ is normalized by the homogeneous result with the mechanical properties of the surface elastic layer, which is the lowest in the soft-coating system and the highest in the hard-coating system. Furthermore, the magnitude of $(\sigma_z^*)_{z=0}^{(1)}$ in the soft-coating system increases with increasing number of elastic layers N, whereas that in the hard-coating system decreases. This result implies that the hard-coating system reduces the magnitude of stress by absorbing force with its soft internal structure.

Figure 5 shows the radial distribution of the normal displacement at the surface layer indented by cylindrical and spherical indenters. $(w_z^*)_{z=0}^{(1)}$ is normalized by the penetration depth ε_0 with respect to the normalized radial distance r/a for the hard- and soft-coating systems. The aspect ratio h/a is fixed at 1.0 and the number of elastic layers $N = 1, 2, 3$, and 4. The results of $(w_z^*)_{z=0}^{(1)}$ for the cylindrical indenter in Fig. 5a are plotted in the range of $1 \leq \quad r/a$ because the normal displacement is equal to the penetration depth in the contact area $0 \leq r/a \leq 1$. Figure 5 indicates that the normal displacement $(w_z^*)_{z=0}^{(1)}$ is insensitive to the mechanical

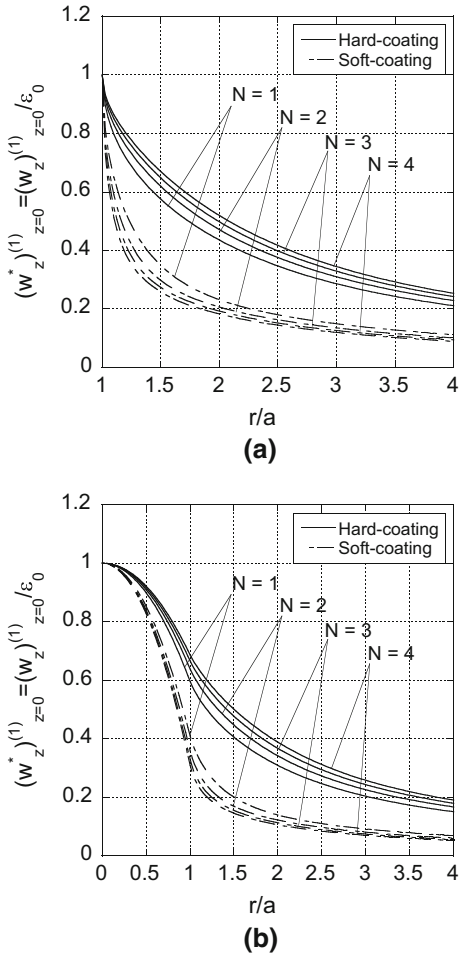

Fig. 5 Radial distribution of $(w_z^*)_{z=0}^{(1)} = (w_z)_{z=0}^{(1)}/\varepsilon_0$ with respect to r/a below **a** flat-ended cylindrical indenter and **b** spherical indenter ($\nu_1 = \cdots = \nu_{N+1} = 0.3, h/a = 1.0$)

properties of the elastic layer and substrate and the number of layers. However, there is a slight difference in $(w_z^*)_{z=0}^{(1)}$ caused by normalization with respect to penetration depth; the actual displacement is thus a function of the mechanical properties and the number of layers. Therefore, the results of $(w_z^*)_{z=0}^{(1)}$ can be applied to indentation tests of multi-layer materials for inverse analysis to determine the mechanical properties of such materials.

Figure 6 shows the variation of the normalized stress singularity factor $S^* = -Sa^{3/2}/P_1$ at the edge of the cylindrical indenter with respect to the aspect ratio h/a for the hard- and soft-coating systems. The number of elastic layers $N = 1$, 2, 3, and 4. The results of the stress singularity factor are expected to be sensitive to the coefficients of the infinite system of simultaneous equations (34) and (37). Therefore, the present results should be compared with the previously reported numerical results to establish their accuracy. As shown in Fig. 6, S^* with a large value of h/a approaches a constant value of $S^* = 1/2\pi^{-1/2}$, which represents the solution for a homogeneous semi-infinite solid with the mechanical properties of the surface layer.

Figure 7 shows the relationships between the normalized axial load $P^* = P/P_1$ and the aspect ratio h/a for the hard- and soft-coating systems indented by cylindrical and spherical indenters. P^* represents the effect of multi-layer system on the semi-infinite solid. Therefore, P^* has a capability as an indentation scaling factor. The number of layers $N = 1$, 2, 3, and 4. Constantinescu et al. [21] provided the numerical results of the apparent contact modulus E^*, which represents a mechanical property of a multi-layer material regarded as one homogeneous layer. They provided symbolic/numerical code for Mathematica (Wolfram Research). The estimation of the apparent contact modulus E^* is based on the calculation of axial load P, and thus, the present results of the normalized axial load are compared with the numerical results obtained using Constantinescu et al.'s Mathematica code, as shown in Fig. 7.

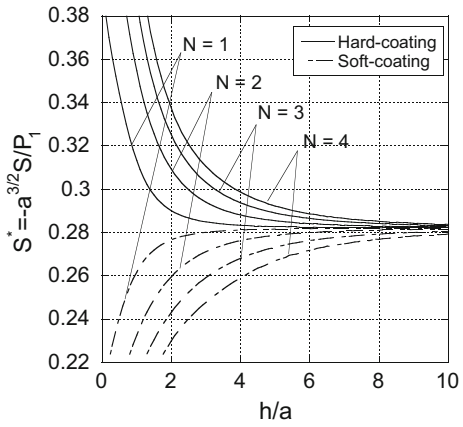

Fig. 6 Variation of $S* = -Sa^{3/2}/P_1$ with respect to h/a below flat-ended cylindrical indenter for various numbers of elastic layers

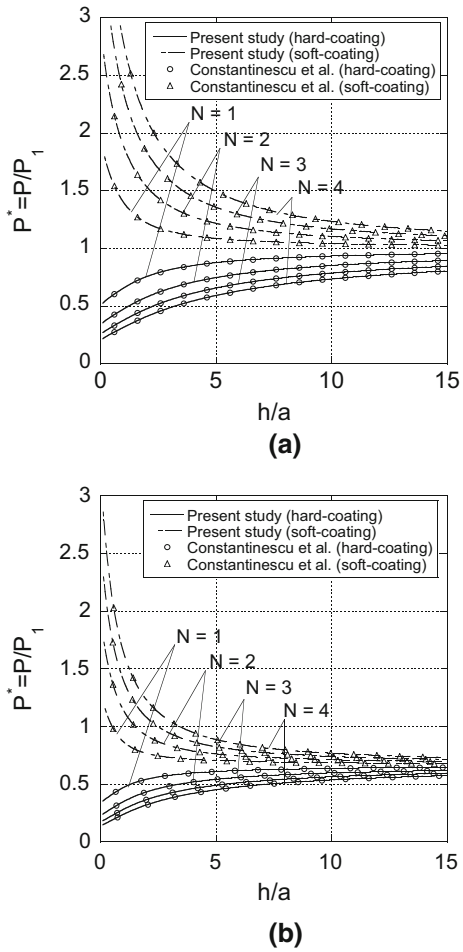

Fig. 7 Relationship between $P^* = P/P_1$ and h/a below **a** flat-ended cylindrical indenter and **b** spherical indenter for various numbers of elastic layers

The present results for the cylindrical and spherical indenters are in good agreement with the reported results. It should be noted that the present results were normalized by contact radius a. Constantinescu et al. [21] predetermined the radius of the indenter R for a spherical indenter and penetration depth d, which is equal to ε_0 in this paper. Contact radius a was determined using iterative calculation in their paper. Therefore, h/a

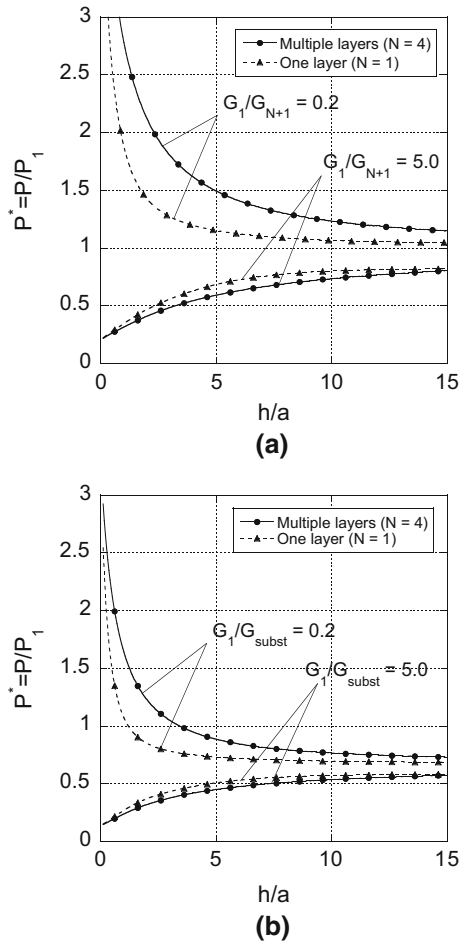

Fig. 8 Comparison of $P^* = P/P_1$ between multiple layers and one layer bonded to an elastic substrate below **a** flat-ended cylindrical indenter and **b** spherical indenter for various numbers of elastic layers

for a spherical indenter was not a predetermined value given by their symbolic/numerical code. A numerical comparison between the present results and those of Constantinescu et al. [21] for various aspect ratios in the range of $h/a < 2$ is given the Appendix.

Figure 8 shows a comparison of the axial load $P^* = P/P_1$ between multiple layers ($N = 4$) and one layer ($N = 1$) with the same shear modulus ratio of the surface layer to the elastic substrate, $G_1/G_{N+1} = 0.2$ and 5.0. The axial load for the multiple layers is higher than that for the one layer when $G_1/G_{N+1} = 0.2$, which represents the soft-coating system, and lower than that for the one layer when$G_1/G_{N+1} = 5.0$, which represents the hard-coating system as shown in Fig. 8. Therefore, the hard-coating multi-layer system effectively protects materials. Furthermore, the effect of multi-layer system has few advantages when the layer thickness becomes sufficiently thin or thick because of the dominant effect of the elastic substrate or surface layer on axial load.

4 Conclusions

The axisymmetric contact problem of a multi-layer coating perfectly bonded to an elastic substrate indented by flat-ended cylindrical and spherical indenters was considered. An analytical solution for an infinite system of simultaneous equations was obtained by using an analytical method that expresses the normal contact stress as an appropriate series with Chebyshev orthogonal polynomials and applying the transfer matrix method, which calculates the transfer matrices derived from the continuous interface condition of an adjacent elastic layer and the substrate. The solution is exact because the analysis procedures did not use any approximation. This paper provides not only the axial load of the rigid indenter but also the distribution of the normal contact stress and displacement of the surface of a multi-layer coating and the stress singularity factor for assessing the

magnitude of the normal contact stress at the edge of a flat-ended cylindrical punch. Numerical results were presented for hard- and soft-coating systems, for which the mechanical properties of each elastic layer and the substrate linearly increase and decrease from the substrate to the top surface layer, respectively. The Poisson's ratios of the elastic layers and substrate were fixed at 0.3 and the elastic layer thicknesses were assumed to be uniform; however, it is possible to change this parameter. The numerical results of axial load for the flat-ended cylindrical and spherical indenters are in good agreement with the results calculated using the Mathematica code provided in a previous study. The numerical results of stress and displacement can serve as guidelines for the design of appropriate mechanical properties of layered materials under indentation loading.

Funding This research did not receive any specific grants from funding agencies in the public, commercial, or not-for-profit sectors.

Compliance with ethical standards

Conflict of interest The authors declare that they have no conflicts of interest.

Appendix

See Tables 3, 4, 5, 6, and 7.

Table 3 Comparison of normalized axial load $P^* = P/P_1$ for various h/a ratios in the range of $h/a > 2.0$ between the present and previously reported results for a cylindrical indenter

h/a	$N = 1$		$N = 2$		$N = 3$		$N = 4$	
	Constantinescu et al.	Present study	Constantinescu et al.	Present study	Constantinescu et al.	Present study	Constantinescu et al.	Present study
Hard coating								
0.5	0.590	0.590	0.414	0.414	0.322	0.322	0.590	0.590
1	0.657	0.657	0.475	0.475	0.378	0.378	0.657	0.657
1.5	0.713	0.713	0.531	0.531	0.430	0.430	0.713	0.713
Soft coating								
0.5	1.589	1.590	2.234	2.237	2.847	2.857	3.436	3.454
1	1.398	1.399	1.884	1.886	2.341	2.345	2.775	2.781
1.5	1.288	1.288	1.672	1.673	2.036	2.037	2.379	2.381

Table 4 Comparison of normalized axial load $P^* = P/P_1$ for various h/a ratios in the range of $h/a < 2.0$ between the present and previously reported results for a spherical indenter ($N = 1$)

h/a	$N = 1$	
	Constantinescu et al.	Present study
Hard coating		
0.49	0.409	0.410
1.00	0.471	0.472
1.49	0.513	0.513
Soft coating		
0.51	0.998	0.997
1.01	0.862	0.864
1.49	0.801	0.802

Table 5 Comparison of normalized axial load $P^* = P/P_1$ with various h/a ratios in the range of $h/a < 2.0$ between the present and previously reported results for a spherical indenter ($N = 2$)

h/a	$N = 2$	
	Constantinescu et al.	Present study
Hard coating		
0.51	0.292	0.292
1.00	0.349	0.349
1.48	0.394	0.395
Soft coating		
0.49	1.395	1.400
1.01	1.130	1.134
1.51	0.997	0.999

Table 6 Comparison of normalized axial load $P^* = P/P_1$ with various h/a ratios in the range of $h/a < 2.0$ between the present and previously reported results for a spherical indenter ($N = 3$)

h/a	$N = 3$	
	Constantinescu et al.	Present study
Hard coating		
0.52	0.230	0.230
0.98	0.280	0.280
1.49	0.327	0.327
Soft coating		
0.48	1.773	1.785
0.99	1.397	1.401
1.51	1.192	1.195

Table 7 Comparison of normalized axial load $P^* = P/P_1$ with various h/a ratios in the range of $h/a < 2.0$ between the present and previously reported results for a spherical indenter ($N = 4$)

h/a	$N = 4$	
	Constantinescu et al.	Present study
Hard coating		
0.47	0.185	0.185
1.01	0.240	0.240
1.48	0.282	0.282
Soft coating		
0.48	2.137	2.146
1.02	1.624	1.628
1.49	1.387	1.389

References

1. Harding, J.W., Sneddon, I.N.: The elastic stresses produced by the indentation of the plane surface of a semi-infinite elastic solid by a rigid punch. Math. Proc. Camb. Philos. Soc. **41**, 16 (1945). https://doi.org/10.1017/S0305004100022325
2. Sneddon, I.N.: The relation between load and penetration in the axisymmetric Boussinesq problem for a punch of arbitrary profile. Int. J. Eng. Sci. **3**, 47–57 (1965). https://doi.org/10.1016/0020-7225(65)90019-4
3. Muki, R.: Asymmetric problems of the theory of elasticity for a semi infinite solid and a thick plate. Prog. Solid Mech. **1**, 399–439 (1960)
4. Lebedev, N.N., Ufliand, I.S.: Axisymmetric contact problem for an elastic layer. J. Appl. Math. Mech. **22**, 442–450 (1958). https://doi.org/10.1016/0021-8928(58)90059-5
5. Hayes, W.C., Keer, L.M., Herrmann, G., Mockros, L.F.: A mathematical analysis for indentation tests of articular cartilage. J. Biomech. **5**, 541–551 (1972). https://doi.org/10.1016/0021-9290(72)90010-3
6. Argatov, I., Daniels, A.U., Mishuris, G., Ronken, S., Wirz, D.: Accounting for the thickness effect in dynamic spherical indentation of a viscoelastic layer: application to non-destructive testing of articular cartilage. Eur. J. Mech. A/Solids **37**, 304–317 (2013). https://doi.org/10.1016/j.euromechsol.2012.07.004
7. Argatov, I.I., Sabina, F.J.: Asymptotic analysis of the substrate effect for an arbitrary indenter. Q. J. Mech. Appl. Math. **66**, 75–95 (2013). https://doi.org/10.1093/qjmam/hbs020

8. Dhaliwal, R.S.: Punch problem for an elastic layer overlying an elastic foundation. Int. J. Eng. Sci. **8**, 273–288 (1970). https://doi.org/10.1016/0020-7225(70)90058-3
9. Yu, H.Y., Sanday, S.C., Rath, B.B.: The effect of substrate on the elastic properties of films determined by the indentation test—axisymmetric boussinesq problem. J. Mech. Phys. Solids **38**, 745–764 (1990). https://doi.org/10.1016/0022-5096(90)90038-6
10. Korsunsky, A.M., Constantinescu, A.: The influence of indenter bluntness on the apparent contact stiffness of thin coatings. Thin Solid Films **517**, 4835–4844 (2009). https://doi.org/10.1016/j.tsf.2009.03.018
11. Keer, L.M., Kim, S.H., Eberhardt, A.W., Vithoontien, V.: Compliance of coated elastic bodies in contact. Int. J. Solids Struct. **27**, 681–698 (1991). https://doi.org/10.1016/0020-7683(91)90028-E
12. Sakamoto, M., Zhu, Q.F., Hara, T.: An axisymmetric contact problem of rigid spheres coated with transversely isotropic layers. Theor. Appl. Mech. Jpn. **44**, 51–62 (1995)
13. Gao, H., Chiu, C.H., Lee, J.: Elastic contact versus indentation modeling of multi-layered materials. Int. J. Solids Struct. **29**, 2471–2492 (1992). https://doi.org/10.1016/0020-7683(92)90004-D
14. Argatov, I.: Frictionless and adhesive nanoindentation: asymptotic modeling of size effects. Mech. Mater. **42**, 807–815 (2010). https://doi.org/10.1016/j.mechmat.2010.04.002
15. Volkov, S., Aizikovich, S., Wang, Y.S., Fedotov, I.: Analytical solution of axisymmetric contact problem about indentation of a circular indenter into a soft functionally graded elastic layer. Acta Mech. Sin. **29**, 196–201 (2013). https://doi.org/10.1007/s10409-013-0022-5
16. Selvadurai, A.P.S., Katebi, A.: An adhesive contact problem for an incompressible non-homogeneous elastic halfspace. Acta Mech. **226**, 249–265 (2015). https://doi.org/10.1007/s00707-014-1171-8
17. Liu, T.J., Wang, Y.S., Xing, Y.M.: Fretting contact of two elastic solids with graded coatings under torsion. Int. J. Solids Struct. **49**, 1283–1293 (2012). https://doi.org/10.1016/j.ijsolstr.2012.02.011
18. Liu, T.J., Wang, Y.S., Xing, Y.M.: The axisymmetric partial slip contact problem of a graded coating. Meccanica **47**, 1673–1693 (2012). https://doi.org/10.1007/s11012-012-9547-0
19. Liu, T.J., Wang, Y.S., Zhang, C.: Axisymmetric frictionless contact of functionally graded materials. Arch. Appl. Mech. **78**, 267–282 (2008). https://doi.org/10.1007/s00419-007-0160-y
20. Liu, T.J., Xing, Y.M.: Analysis of graded coatings for resistance to contact deformation and damage based on a new multi-layer model. Int. J. Mech. Sci. **81**, 158–164 (2014). https://doi.org/10.1016/j.ijmecsci.2014.02.009
21. Constantinescu, A., Korsunsky, A.M., Pison, O., Oueslati, A.: Symbolic and numerical solution of the axisymmetric indentation problem for a multilayered elastic coating. Int. J. Solids Struct. **50**, 2798–2807 (2013). https://doi.org/10.1016/j.ijsolstr.2013.04.017
22. Wei, Y., Ji, Y., Weiqiu, C.: A three-dimensional solution for laminated orthotropic rectangular plates with viscoelastic interfaces. Acta Mech. Solida Sin. **19**, 181–188 (2006). https://doi.org/10.1007/s10338-006-0622-8
23. Ai, Z.Y., Zhang, Y.F.: The analysis of a rigid rectangular plate on a transversely isotropic multilayered medium. Appl. Math. Model. **39**, 6085–6102 (2015). https://doi.org/10.1016/j.apm.2015.01.054
24. Stan, G., Adams, G.G.: Adhesive contact between a rigid spherical indenter and an elastic multi-layer coated substrate. Int. J. Solids Struct. **87**, 1–10 (2016). https://doi.org/10.1016/j.ijsolstr.2016.02.043
25. Zhang, H., Wang, W., Zhang, S., Zhao, Z.: Semi-analytical solution of three-dimensional steady state thermoelastic contact problem of multilayered material under friction heating. Int. J. Therm. Sci. **127**, 384–399 (2018). https://doi.org/10.1016/j.ijthermalsci.2018.02.006
26. Miura, K., Sakamoto, M., Kobayashi, K.: Analytical solution of axisymmetric indentation of an elastic layer-substrate body. Theor. Appl. Mech. Jpn. **64**, 81–101 (2018)
27. Miura, K., Sakamoto, M., Kobayashi, K., Pramudita, J.A., Tanabe, Y.: An analytical solution for the axisymmetric problem of a penny-shaped crack in an elastic layer sandwiched between dissimilar materials. Mech. Eng. J. **5**, 18-00125–18–00125 (2018). https://doi.org/10.1299/mej.18-00125
28. Love, A.E.H.: A Treatise on the Mathematical Theory of Elasticity. Cambridge University Press, Cambridge (1927)
29. Bateman, H.: Tables of Integral Transforms. McGraw-Hill, New York (1954)
30. Moriguchi, S., Udagawa, K., Hitomatsu, S.: Mathematical Formulas, vol. 3. Iwanami, Tokyo (1987). **(in Japanese)**